Combustion Theory and Modelling, 2020
Vol. 24, No. 2, 245–261, https://doi.org/10.1080/13647830.2019.1674923

Numerical studies on autoignition and detonation development from a hot spot in hydrogen/air mixtures

Yuan Gao[a†], Peng Dai[b] and Zheng Chen [a,c*]

[a]*SKLTCS, CAPT, College of Engineering, Peking University, Beijing, People's Republic of China;* [b]*Department of Mechanics and Aerospace Engineering, Southern University of Science and Technology, Shenzhen, People's Republic of China;* [c]*Beijing Innovation Center for Engineering Science and Advanced Technology, Peking University, Beijing, People's Republic of China*

(*Received 4 June 2019; accepted 20 September 2019*)

Detonation development inside spark ignition engines can result in the so called super-knock with extremely high pressure oscillation above 200 atm. In this study, numerical simulations of autoignitive reaction front propagation in hydrogen/air mixtures are conducted and the detonation development regime is investigated. A hot spot with linear temperature distribution is used to induce autoignitive reaction front propagation. With the change of temperature gradient or hot spot size, three typical autoignition reaction front modes are identified: supersonic reaction front; detonation development and subsonic reaction front. The effects of initial pressure, initial temperature, fuel type and equivalence ratio on detonation development regime are examined. It is found that the detonation development regime strongly depends on mixture composition (fuel and equivalence ratio) and thermal conditions (initial pressure and temperature). Therefore, to achieve the quantitative prediction of super-knock in engines, we need use the detonation development regime for specific fuel at specific initial temperature, initial pressure, and equivalence ratio.

Keywords: detonation development; autoignitive reaction front; hydrogen/air; temperature gradient

1. Introduction

Engine knock is one of the main constrains for the development of high-efficiency spark ignition engines (SIEs). It is generally accepted that knock in SIEs is related to end-gas autoignition [1,2]. End-gas autoignition can generate pressure oscillation around 20 atm which is referred to as the normal knock. Recently, the so called super-knock with extremely high pressure oscillation above 200 atm has been observed in highly boosted SIEs and rapid compression machines [3–9]. Such high pressure in super-knock was attributed to detonation development [4,6–8].

According to the SWACER (shock-wave amplification by coherent energy release) mechanism [10] and reactivity gradient theory [11], detonation development can be induced by a hot spot. In a combustible mixture at high temperature and pressure, a hot spot can generate autoignitive reaction front propagation. When the reaction front propagation speed is close to the local sound speed, the coherent coupling between chemical

*Corresponding author. Email: cz@pku.edu.cn
†Current at West Virginia University, USA.

reaction and pressure wave occurs and it might result in a developing detonation [11,12]. In the literature, there are many studies on detonation development from a hot spot (e.g. Refs. [13–20]). However, the critical conditions for this kind of detonation development were not quantified in these studies.

For the first time, Bradley and coworkers [12,21] proposed a detonation peninsula which quantifies the detonation development regime based on the following two non-dimensional parameters:

$$\xi = \frac{\mathrm{d}T_0}{\mathrm{d}r} \Big/ \left(\frac{\mathrm{d}T_0}{\mathrm{d}r}\right)_c, \quad \varepsilon = \frac{r_0/a}{\tau_e}, \tag{1}$$

where $\mathrm{d}T_0/\mathrm{d}r$ and r_0 are respectively the temperature gradient and radius of the hot spot with a linear temperature distribution; $(\mathrm{d}T_0/\mathrm{d}r)_c$ is the critical temperature gradient at which the reaction front propagation speed, u_a, is equal to the local sound speed, a; and τ_e is the excitation time defined as the time interval between 5% and maximum heat release rate [12]. The critical temperature gradient is defined as [12,21]:

$$\left(\frac{\mathrm{d}T_0}{\mathrm{d}r}\right)_c = \left(a\frac{\mathrm{d}\tau_i}{\mathrm{d}T_0}\right)^{-1}. \tag{2}$$

According to Zeldovich's theory [11], the propagation speed of the hot spot-induced autoignitive front is inversely proportional to the gradient of the ignition delay time:

$$u_a = \left(\frac{\mathrm{d}\tau_i}{\mathrm{d}r}\right)^{-1} = \left(\frac{\mathrm{d}\tau_i}{\mathrm{d}T_0} \cdot \frac{\mathrm{d}T_0}{\mathrm{d}r}\right)^{-1}. \tag{3}$$

Substituting Equation (2) into Equation (3) indicates that $u_a = a$ at the critical temperature gradient. It can be shown that the first non-dimensional parameter, ξ, in Equation (1) is equal to the ratio between the local sound speed and the reaction front propagation speed, i.e. $\xi = a/u_a$ [12]. The second parameter, ε, represents the ratio between acoustic time and heat release time. As schematically shown in the plot of ξ versus ε in Figure 1, there are five modes for the autoignitive reaction front propagation. These modes are classified according to the comparison among the reaction front propagation speed, u_a, the sound speed, a, and the laminar flame speed, S_u [11,12], as described in Figure 1.

Regime III in the plot of ξ–ε was adopted by Bradley and Kalghatgi [22,23] and Rudloff *et al.* [24] to quantify the critical conditions for detonation development and engine knock. Three-dimensional LES (Large Eddy Simulation) performed by Robert *et al.* [25] showed that the detonation development regime proposed by Bradley and coworkers [12,21] can be used to quantify the super-knock phenomenon in SIEs. However, Bradley's detonation regime/peninsula was originally determined based on simulations for syngas/air mixtures [12,21]. Though Bates *et al.* [26] showed that Bradley's detonation peninsula also works for iso-octane, recent studies [27–31] indicated that the detonation development regime in terms of ξ and ε might depend on thermal conditions (initial temperature and pressure) and mixture composition (fuel, equivalence ratio, dilutions). Though the parameters ξ and ε depend upon the state of the mixture, the effect of the state of the mixture on detonation development cannot be captured in the ξ–ε diagram. Moreover, besides the ignition delay time, excitation time, and critical temperature gradient, the volumetric energy density (which affects detonation development and is not included in the parameters ξ and ε) also depends on thermal conditions and mixture composition. Therefore, the relevant

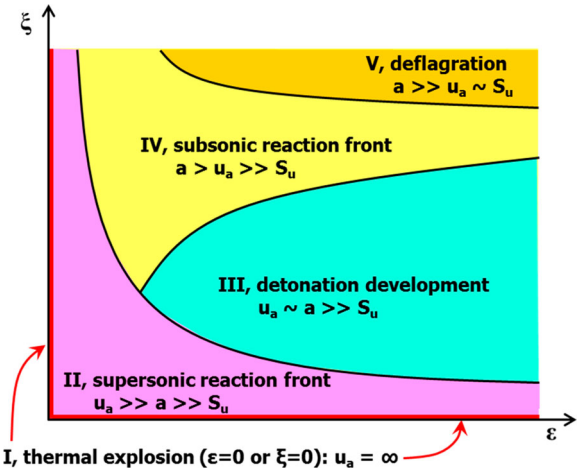

Figure 1. Schematics of different regimes of autoignitive reaction front propagation induced by a hot spot (adapted from [22]). Five modes, I–V, and the comparison among different speeds are shown.

parametric domain for detonation development is expected to be broader than that can be described in the ξ–ε plane.

Therefore, further study is needed to understand how thermal conditions and mixture composition affect the detonation development regime. This motivates the present study. The objectives of this study are to obtain the detonation development regimes for some fuel other than syngas and to examine the effects of initial pressure, initial temperature and equivalence ratio on detonation development regime. Since hydrogen is the simplest fuel with well-established and smallest chemical mechanism, it is considered in this work.

2. Numerical model and methods

We consider the autoignitive reaction front propagation induced by a hot spot in hydrogen/air mixtures. Spherical symmetry is assumed and the model is one-dimensional in a spherical coordinate. The hot spot is located at the centre and it is represented by the initial linear temperature distribution:

$$T(t=0,\, r) = \begin{cases} T_0 + (r - r_0)\frac{\mathrm{d}T_0}{\mathrm{d}r} & \text{for } 0 \le r \le r_0 \\ T_0 & \text{for } r_0 \le r \le R_W \end{cases} \tag{4}$$

where t and r are respectively the temporal and spatial coordinates. The spherical chamber radius is fixed to be $R_W = 5$ cm. The hot spot size, r_0, the temperature gradient, $\mathrm{d}T_0/\mathrm{d}r$, and the initial temperature of the mixture outside of the hot spot, T_0, are to be specified. The computational domain is initially filled with a static hydrogen/air mixture with uniformly distributed pressure and equivalence ratio. It is noted that though only temperature gradient is considered here, the concentration gradient may also result in different autoignition modes including detonation development [32–34].

The transient autoignitive reaction front propagation from a hot spot is simulated using A-SURF (Adaptive Simulation of Unsteady Reactive Flow) [35–37]. Finite volume

method is used to solve the species, momentum and energy conservation equations for 1-D, adiabatic, multi-component, compressible, reactive flow in a spherical coordinate:

$$\frac{\partial U}{\partial t} + \frac{\partial F(U)}{\partial r} + 2\frac{G(U)}{r} = F_v(U) + S_R, \tag{5}$$

where t is the temporal coordinate. The vectors U, $F(U)$, $G(U)$, $F_v(U)$, and S_R are defined as:

$$U = \begin{pmatrix} \rho Y_1 \\ \rho Y_2 \\ \vdots \\ \rho Y_n \\ \rho u \\ E \end{pmatrix}, F(U) = \begin{pmatrix} \rho u Y_1 \\ \rho u Y_2 \\ \vdots \\ \rho u Y_n \\ \rho u^2 + P \\ (E+P)u \end{pmatrix}, G(U) = \begin{pmatrix} \rho u Y_1 \\ \rho u Y_2 \\ \vdots \\ \rho u Y_n \\ \rho u^2 \\ (E+P)u \end{pmatrix},$$

$$F_v(U) = \begin{pmatrix} -r^{-2}(r^2 \rho Y_1 V'_1)_r \\ -r^{-2}(r^2 \rho Y_2 V'_2)_r \\ \vdots \\ -r^{-2}(r^2 \rho Y_n V'_n)_r \\ r^{-2}(r^2 \tau_1)_r - 2\tau_2/r \\ r^{-2} q_r + \Phi \end{pmatrix}, S_R = \begin{pmatrix} \omega_1 \\ \omega_2 \\ \vdots \\ \omega_n \\ 0 \\ 0 \end{pmatrix} \tag{6}$$

where ρ, u and E are the density, radial flow velocity and total energy per unit mass, respectively. The subscript r in $F_v(U)$ stands for the partial derivative with respect to r. Y_k, ω_k and V'_k are the mass fraction, production rate and diffusion velocity of species k, respectively. The production rate ω_k is specified via the collection of elementary reactions and it is calculated using the CHEMKIN package [38]. The mixture-averaged method is employed to calculate species diffusion velocity. Instead of solving the continuity equation, the species conservation equations for all n species are solved in A-SURF. The continuity equation is recovered from the summation of all species conservation equations.

In the momentum equation, P is the pressure and the viscous stresses, τ_1 and τ_2, are respectively:

$$\tau_1 = 2\mu\frac{\partial u}{\partial r} - \frac{2}{3}\mu\frac{1}{r^2}\frac{\partial (r^2 u)}{\partial r}, \quad \tau_2 = 2\mu\frac{u}{r} - \frac{2}{3}\mu\frac{1}{r^2}\frac{\partial (r^2 u)}{\partial r}, \tag{7}$$

where μ is the dynamic viscosity of the mixture.

In the energy conservation equation, the total energy, E, is defined through

$$E = -P + \rho u^2/2 + \rho h,\ h = \sum_{k=1}^{n} (Y_k h_k),\ h_k = h_{k,0} + \int_{T_0}^{T} C_{P,k}(T)\mathrm{d}T, \tag{8}$$

where T is the temperature, h_k, the enthalpy of species k, $h_{k,0}$ the species enthalpy of formation at the reference temperature T_0, and $C_{P,k}$ the specific heat of species k at constant pressure. The heat flux is

$$q = r^2 \left[\lambda \frac{\partial T}{\partial r} - \rho \sum_{k=1}^{n} (h_k Y_k V'_k) \right], \tag{9}$$

where λ is the thermal conductivity of the mixture.

In addition, the viscous dissipation rate is

$$\Phi = \mu \left\{ 2\left(\frac{\partial u}{\partial r}\right)^2 + 4\left(\frac{u}{r}\right)^2 - \frac{2}{3}\left[\frac{1}{r^2}\frac{\partial (r^2 u)}{\partial r}\right]^2 \right\} + u\left[\frac{1}{r^2}\frac{\partial (r^2 \tau_1)}{\partial r} - 2\frac{\tau_2}{r}\right]. \tag{10}$$

The pressure can be obtained from the density, temperature and mean molecular weight using the equation of state for an ideal gas:

$$P = \rho RT/\bar{M}, \tag{11}$$

where $R = 8.314$ J/(mol K) is the universal gas constant.

The thermodynamic and transport properties in Equations (5)–(11) are evaluated using the CHEMKIN and TRANSPORT packages [38] interfaced with A-SURF.

In A-SURF, the finite volume method is used to discretise the governing Equation (5). The second-order accurate, Strang splitting fractional-step procedure is utilised to separate the time evolution of the stiff reaction term S_R from that of the convection and diffusion terms. In the first fractional step, the non-reactive flow is solved and the Runge–Kutta, MUSCL-Hancock, and central difference schemes, all of second-order accuracy, are employed for the calculation of the temporal integration, convective flux, and diffusive flux, respectively. In the second fractional step, the chemistry term is solved using the VODE solver [39]. To efficiently resolve the autoignition and reaction front propagation processes, a multi-level adaptive mesh refinement algorithm is used in A-SURF. The propagating reaction zone, pressure/shock wave and detonation wave are always covered by the finest mesh with the width of 2 µm. The time step used for explicit integration is 0.4 ns. Grid convergence is achieved as demonstrated in [27,37,40]. A-SURF has been used in previous studies on ignition, premixed flame propagation and detonation initiation (e.g. [41–49]).

According to the autoignition model used in this study, adiabatic, non-penetrative, reflective boundary conditions are adopted for both boundaries at $r = 0$ and $r = R_W$:

$$u = 0, \quad \frac{\partial T}{\partial r} = \frac{\partial Y_k}{\partial r} = \frac{\partial P}{\partial r} = 0. \tag{12}$$

According to Equation (12), the linear temperature distribution in Equation (4) in fact starts at $r = r_c$ (half width of the mesh) rather than $r = 0$. Since the region around $r = 0$ is always covered by the finest mesh with the width of 2 µm, we have $r_c = 1$ µm which is negligible compared to the hot spot size r_0.

Libermann and coworkers [50–52] found that compared to the detailed chemical mechanism, simplified one-step or two-step chemical models cannot quantitatively reproduce the autoignitive front propagation from a hot spot. Therefore, the detailed mechanism for hydrogen oxidation should be used. In the literature, there are several detailed mechanisms developed for hydrogen/air mixtures, including those by Li *et al.* [53], Burke *et al.* [54], Keromnes *et al.* [55] and Alekseev *et al.* [56]. These four mechanisms are used to calculate the ignition delay time, excitation time and critical temperature gradient for hydrogen/air mixtures at different initial temperatures, pressures and equivalence ratios. The constant-volume homogeneous ignition process is simulated, from which the ignition delay time and excitation time are obtained. The critical temperature gradient is obtained according to its definition in Equation (2). Figure 2 shows that these four detailed mechanisms predict nearly the same results for stoichiometric hydrogen/air mixtures at $P_0 = 40$ atm.

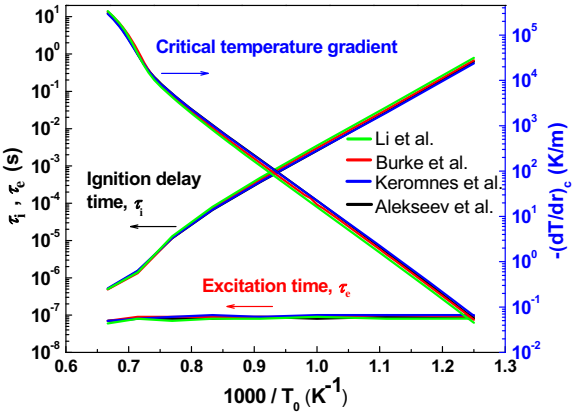

Figure 2. Change of the ignition delay time, τ_i, the excitation time, τ_e, and the critical temperature gradient – $(\mathrm{d}T/\mathrm{d}r)_c$, with the initial temperature, T_0, for stoichiometric hydrogen/air mixture at $\phi = 1.0$ and $P_0 = 40$ atm. The results predicted by four mechanisms [53–56] are plotted together for comparison.

Results for other values of equivalence ratio and initial pressure are also obtained; and very good agreement is also achieved for results predicted by these four mechanisms. Therefore, in the following here we only use the mechanism developed by Keromnes *et al.* [55]. Similar results are expected if other detailed hydrogen mechanisms are used.

3. Results and discussion

3.1. *Autoignition in homogeneous hydrogen/air mixtures*

The ignition delay time, τ_i, and excitation time, τ_e, are the two most important parameters to characterise the autoignition and heat release duration in a homogeneous mixture. They are obtained from simulation of the constant-volume homogeneous ignition process. Figure 3 shows the change of τ_i and τ_e with the initial temperature for hydrogen/air mixtures at different pressures and equivalence ratios. Besides, Figure 3 also shows the critical temperature gradient $(\mathrm{d}T/\mathrm{d}r)_c$.

Both the ignition delay time and critical temperature gradient are shown to be strongly affected by the initial temperature. Though the influence of the initial pressure and equivalence ratio is relatively weaker compared to the initial temperature, quantitative effects of the initial pressure and equivalence ratio on τ_i, τ_e and $(\mathrm{d}T/\mathrm{d}r)_c$ are still observed. For example, the excitation time is shown to be shorter at higher initial pressure and for stoichiometric composition. With the increase of initial pressures, the ignition delay is shown to be shorter (longer) for $T_0 < 1200$ K ($T_0 > 1200$ K). This is due to the fact that the reaction rates of the branching reactions, $\mathrm{H} + \mathrm{O_2} = \mathrm{O} + \mathrm{OH}$ and $\mathrm{H_2O_2} + \mathrm{M} = \mathrm{OH} + \mathrm{OH} + \mathrm{M}$, and the termination reaction, $\mathrm{H} + \mathrm{O_2} + \mathrm{M} = \mathrm{HO_2} + \mathrm{M}$, strongly depend on the pressure [57]. Besides, the volumetric energy density (which determines the strength of the pressure pulse induced by local autoignition) strongly depends on the initial pressure, initial temperature and equivalence ratio [27,30,58]. Therefore, it is expected that the detonation development regime is affected by the initial pressure, initial temperature and equivalence ratio. This will be discussed in Sub-section 3.3.

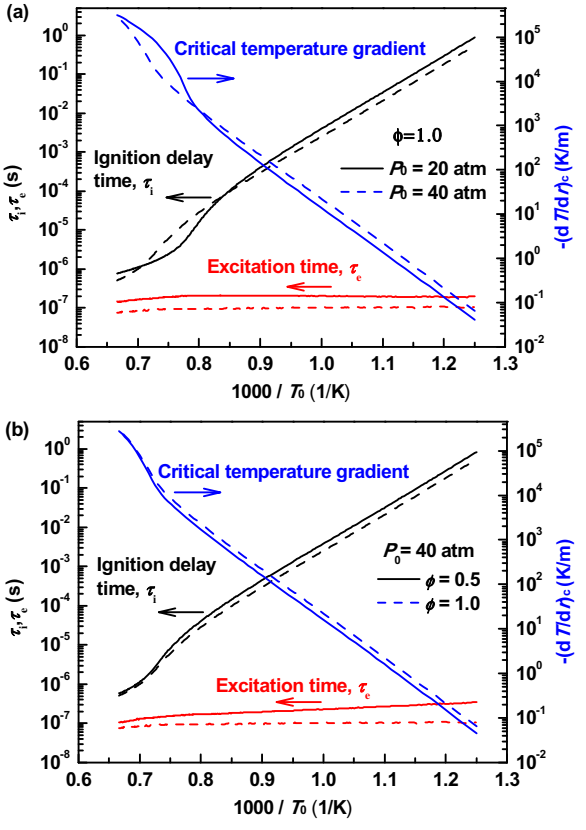

Figure 3. Change of the ignition delay time, τ_i, the excitation time, τ_e, and the critical temperature gradient – $(\mathrm{d}T/\mathrm{d}r)_c$, with the initial temperature, T_0, for hydrogen/air mixtures at: (a) different pressures of $P_0 = 20$ atm (solid lines) and $P_0 = 40$ atm (dashed lines); (b) different equivalence ratios of $\phi = 0.5$ (solid lines) and $\phi = 1.0$ (dashed lines).

3.2. *Typical modes of autoignitive reaction front propagation*

We first consider the typical modes of autoignitive reaction propagation as shown in Figure 1. Mode I, thermal explosion, corresponds to the homogenous ignition (either $\mathrm{d}T_0/\mathrm{d}r = 0$ or $r_0 = 0$ in Equation (1)) and it is considered in the previous sub-section. In SIEs, the unburned gas is compressed to relatively high temperature and pressure. Therefore, Mode V, deflagration, corresponds to premixed flame propagation in a mixture with high initial temperature and pressure. At normal temperature and pressure, the ignition delay of the unburned mixture is infinitely large and the laminar flame speed is well-defined by the eigenvalue problem. However, at high temperature and pressure as in SIEs, the ignition delay of unburned mixture might be the same order of the characteristic flame time (e.g. the ratio between flame thickness and flame speed). Consequently, strong interaction or competition between autoignition and flame propagation could occur. Recently, mode V has received great attention since it is related to premixed flame propagation in advanced SIEs [59–64] and end-gas autoignition [65–69]. Here we focus on modes II–IV since they determine the boundaries for the detonation development as shown in Figure 1

Table 1. Typical cases of autoignitive reaction front propagation in a stoichiometric H_2/air mixture at $T_0 = 1000$ K and $P_0 = 40$ atm.

Case	dT_0/dr (K/mm)	r_0 (mm)	ξ	ε	Mode
1. (a)	− 0.025	1.5	1	20.1	II, supersonic reaction front
1. (b)	− 0.38	1.5	15	20.1	III, detonation development
1. (c)	− 1.07	1.5	42	20.1	IV, subsonic reaction front
1. (d)	− 1.06	0.37	42	5.0	III, detonation development
1. (e)	− 1.06	0.2	42	2.7	II, supersonic reaction front

Here we first consider the stoichiometric hydrogen/air mixture with $T_0 = 1000$ K and $P_0 = 40$ atm. In the next sub-section, we will consider different initial pressure of $P_0 = 20$ atm, initial temperature of $T_0 = 1200$ K, and equivalence ratio of $\phi = 0.5$ so that their effects on detonation development regime can be examined.

Five typical cases are listed in Table 1. The first three cases, (a)–(c), correspond to different values of ξ but the same value of ε; while the last three cases, (c)–(e), correspond to different values of ε but the same value of ξ. From case (a) to case (c), the magnitude of the temperature gradient increases while the hot spot size is fixed to be $r_0 = 1.5$ mm. From case (c) to case (e), the hot spot size decreases while the temperature gradient remains nearly constant. The mode of autoignitive reaction front propagation for each case is listed in Table 1.

Figure 4 shows the temporal evolution of temperature, pressure and heat release rate distributions for cases (a)–(e). For case (a) with very small temperature gradient, the difference in the temperature at the centre and that of the ambient mixture is only 0.04 K. The whole mixture reaches around 1400 K and 55 atm at $t = 2575.61$ μs (line #1 in Figure 4(a)). Then the small temperature difference results in earlier thermal runaway at the centre (line #2) and an outwardly propagating autoignitive reaction front (lines #2 to #3). As shown in Figure 5, the reaction front speed for case (a) is always above 3000 m/s, which is larger than the CJ detonation speed and much larger than the sound speed. Therefore, the chemical reaction cannot couple with the pressure wave and there is no detonation development, which makes case (a) correspond to supersonic reaction front propagation (i.e. mode II). Similarly, case (e) with a small hot spot size of $r_0 = 0.2$ mm also belongs to model II of supersonic reaction front. For both cases (a) and (e), the final temperature and pressure approaches to the equilibrium values around 3200 K and 110 atm, respectively.

Figure 4(b) shows that detonation development occurs for case (b). Detonation wave propagation in the range of $0.2 < R_f < 0.4$ cm is clearly observed. The peak pressure is around 240 atm, which is much higher than the equilibrium pressure. Besides, Figure 5 shows that for case (b), the reaction front propagates at a constant speed very close to the CJ value of 1991 m/s for $2 < R_f < 4$ mm. A similar trend is also observed for case (d) in Figure 4(d) and Figure 5. Therefore, both cases (b) and (d) correspond to mode III of detonation development. Such detonation development is caused by the coherent coupling between chemical reaction and pressure wave [16], and it can be interpreted by the SWACER mechanism [10] and reactivity gradient theory [11].

A typical case of mode IV, subsonic reaction front, is shown in Figure 4(c). The pressure is nearly uniformly distributed in the whole domain before the thermal explosion occurs throughout the unburned mixture on the right side (line #4 in Figure 4(c)). Figure 5

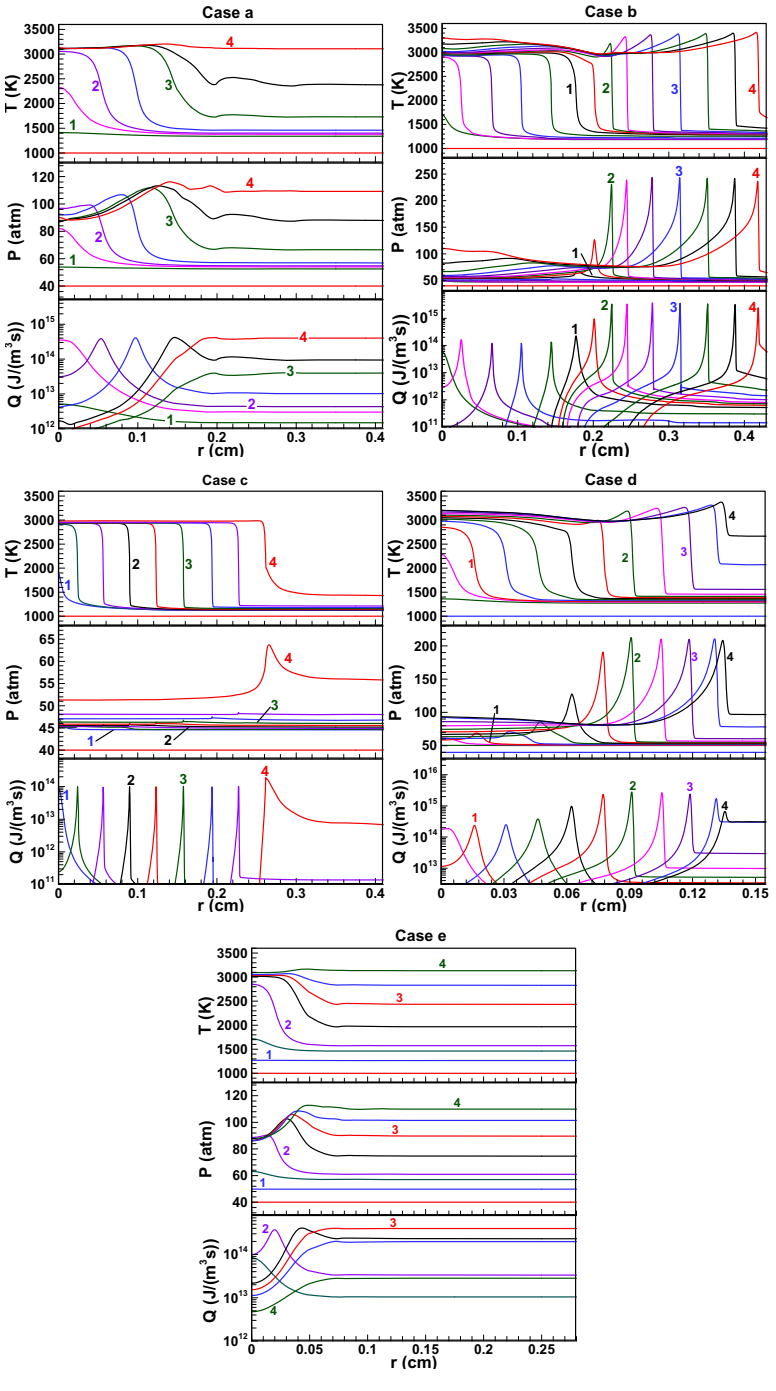

Figure 4. Temporal evolution of temperature, pressure and heat release rate distributions during the autoignitive reaction front propagation induced by a hot spot for cases a–e listed in Table 1. The time sequence for case a is 1: 2575.61 μs, 2: 2575.93 μs, 3: 2576.17 μs, 4: 2576.27 μs; that for case b is 1: 2574.50 μs, 2: 2574.87 μs, 3: 2575.35 μs, 4: 2575.91 μs; that for case c is 1: 2545.81 μs, 2: 2553.78 μs, 3: 2562.20 μs, 4: 2575.77 μs; that for case d is 1: 2575.22 μs, 2: 2575.96 μs, 3: 2576.12 μs, 4: 2576.21 μs; and that for case e is 1: 2574.30 μs, 2: 2576.13 μs, 3: 2576.21 μs, 4: 2576.29 μs.

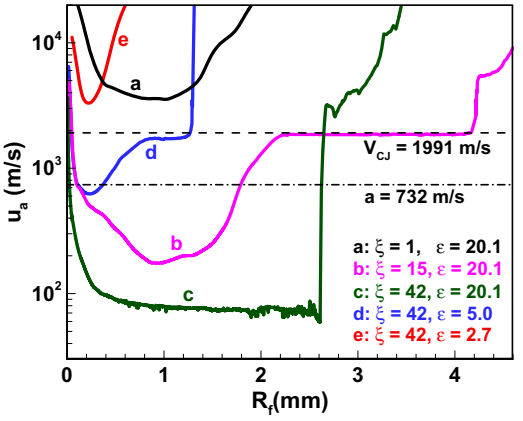

Figure 5. Reaction front propagation speed as a function of its location for different values of ξ and ε. The mixture is stoichiometric H_2/air at $T_0 = 1000\,\mathrm{K}$ and $P_0 = 40\,\mathrm{atm}$. The CJ detonation speed ($V_{\mathrm{CJ}} = 1991\,\mathrm{m/s}$) and sound speed ($a = 732\,\mathrm{m/s}$) are denoted by the horizontal dashed and dash-dotted lines, respectively.

shows that for case (c), the reaction front propagates at a speed around 80 m/s until the abrupt increase due to the thermal explosion. As shown in the previous study [32], the subsonic reaction front is affected by molecular diffusion (mass diffusion and heat conduction).

3.3. *The detonation development regime*

Figure 6 shows the detonation development regime III in the plot of ξ against ε for the stoichiometric hydrogen/oxygen mixture at $T_0 = 1000\,\mathrm{K}$ and $P_0 = 40\,\mathrm{atm}$. The maximum pressure is shown. The five cases, (a)–(e), discussed in the previous sub-section are also marked in Figure 6. It is difficult to accurately determine the boundaries between mode

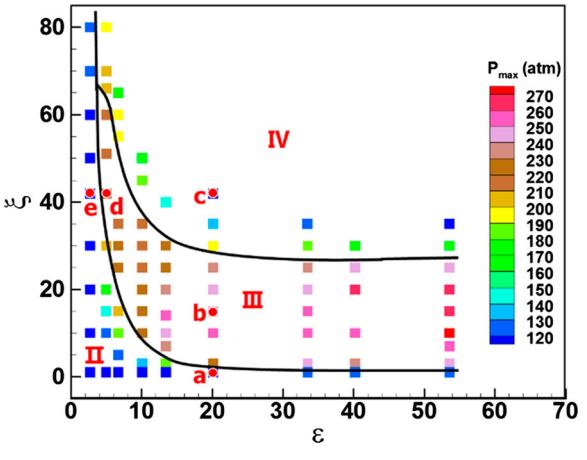

Figure 6. Maximum pressure and detonation regime in the ξ–ε diagram for stoichiometric H_2/air mixture at $T_0 = 1000\,\mathrm{K}$ and $P_0 = 40\,\mathrm{atm}$. Three modes of reaction front propagation: II, supersonic reaction front; III, detonation development; and IV, subsonic reaction front.

III and II or IV since there is no quantitative criteria to judge whether detonation development occurs or not. In this study, detonation development is considered to occur when the following two quantitative criteria are both satisfied: (1) the maximum pressure is at least two times of the equilibrium pressure; and (2) the reaction front propagation speed reaches at least 90% of the C–J detonation speed. A 'Rhino-Horn' shaped detonation development regime, III, is shown in Figure 6. This is different from the traditional detonation development regime shown in Figure 1. Specifically, detonation development is usually easier to happen for larger hot spot size or smaller excitation time (i.e. larger value of ε). However, Figure 6 shows that with the increase of ε, the detonation development can be suppressed and the mode changes from III of detonation development (for case d) to IV of subsonic reaction front (for case c). Such abnormal trend has been observed only for hydrogen while the traditional detonation development regime (similar to that in Figure 1) is observed for other fuels. This reason for such abnormal behaviour is still not clear and it deserves further study.

It is noted that the detonation regime in Figure 6 is greatly different from the detonation peninsular which was determined for syngas/air mixtures by Bradley and coworkers [12,21]. Figure 7 shows the detonation regimes of different fuels including hydrogen (this work), syngas [12,21], n-heptane [27], and dimethyl ether (DME) [27]. Significant qualitative and quantitative differences are observed among the detonation regimes of these fuels. Therefore, the detonation development regime strongly depends on fuel. This conclusion is consistent with previous studies [27,30,31]. Besides, it is observed that for DME, the detonation development regime also depends on the temperature. In the following, the effects of thermal conditions and equivalence ratio on the detonation development regime are assessed for hydrogen/air mixtures.

Besides the above reference condition with $P_0 = 40$ atm, $T_0 = 1000$ K and $\phi = 1.0$, we also consider initial pressure of $P_0 = 20$ atm, initial temperature of $T_0 = 1200$ K, and equivalence ratio of $\phi = 0.5$. The corresponding detonation development regimes

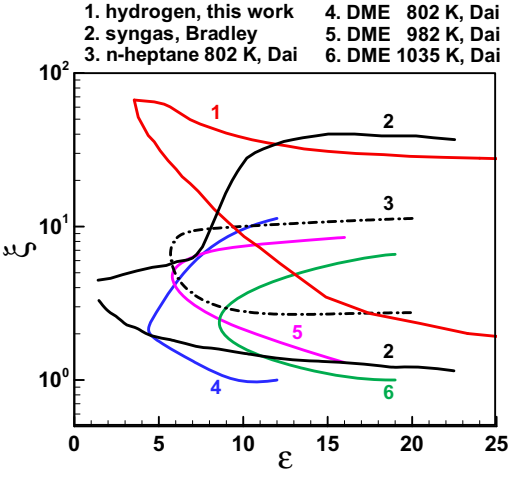

Figure 7. The detonation regime in the ξ–ε diagram for different fuel/air mixtures: (1) H_2/air (this work), $\phi = 1.0$, $T_0 = 1000$ K and $P_0 = 20$ atm; (2) H_2/CO/air, 50% H_2-50% CO–air (Bradley *et al.* [12, 21]), $\phi = 1.0$, $T_0 = 1000$ K and $P_0 = 50$ atm; (3) n-heptane/air (Dai *et al.* [27]), $\phi = 1.0$, $T_0 = 802$ K and $P_0 = 40$ atm; (4) DME/air (Dai *et al.* [27]), $\phi = 1.0$, $T_0 = 802$, 982 and 1035 K and $P_0 = 40$ atm.

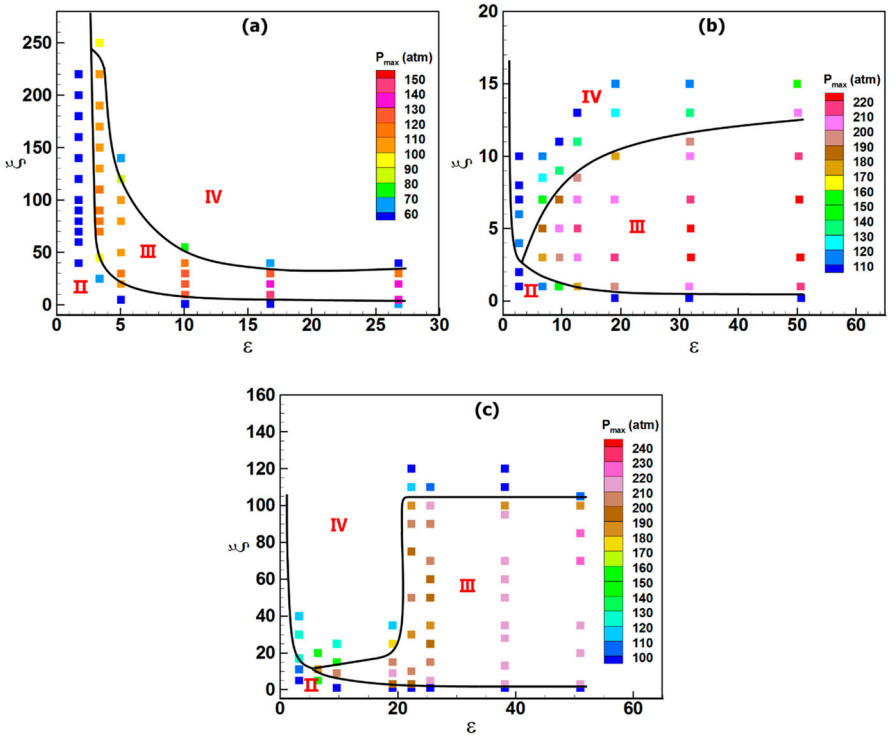

Figure 8. Maximum pressure and detonation regime in the ξ–ε diagram for H_2/air mixtures at (a) $\phi = 1.0$, $T_0 = 1000$ K and $P_0 = 20$ atm; (b) $\phi = 1.0$, $T_0 = 1200$ K and $P_0 = 40$ atm; and (c) $\phi = 0.5$, $T_0 = 1000$ K, $P_0 = 40$ atm.

are plotted in Figure 8; and the comparison with the reference condition ($P_0 = 40$ atm, $T_0 = 1000$ K and $\phi = 1.0$) is depicted in Figure 9.

Comparison among these regime maps indicates that the initial temperature, initial pressure, and equivalence ratio all greatly affect the detonation development regime. It is observed that the detonation development regimes in the ξ–ε plot are similar for initial pressures of 40 and 20 atm. This indicates that the initial pressure has a relatively weak influence on the detonation development regime. With the increase of the initial temperature from 1000 to 1200 K, the energy density of the mixture decreases. Therefore, the upper bound of detonation development regime moves downwardly and a C-shaped detonation development regime is observed in Figure 8(b). The comparison in Figure 9(b) indicates that the detonation regime becomes much narrower at higher initial temperature. When the equivalence ratio decreases from 1.0 to 0.5, a much wider detonation development regime is obtained and it is similar to the detonation peninsula proposed by Bradley and coworkers [12,21] for syngas/air mixtures.

Figures 8 and 9 show that under different initial conditions, different shapes of detonation regime can be observed including peninsula, C-shape and Rhino-Horn shape. Therefore, the initial conditions play an important role in the formation of a detonation regime, and we cannot use the same detonation development regime map for different initial conditions and different mixtures. It is noted that the reason for the change in the shape of the detonation regime with the initial thermal conditions (pressure and temperature) and

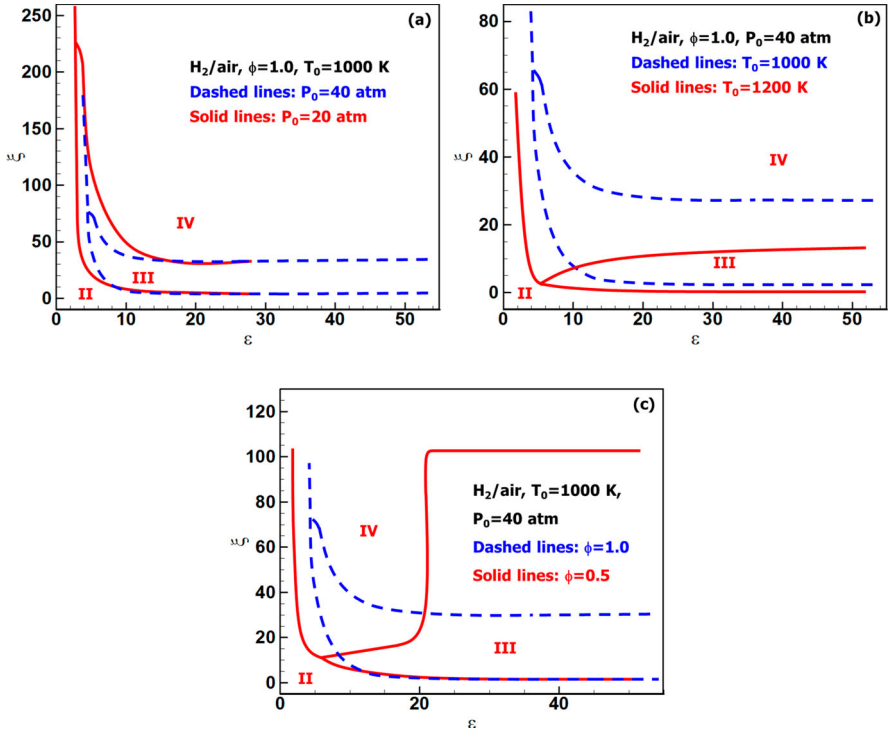

Figure 9. Effects of (a) initial pressure, (b) initial temperature, and (c) equivalence ratio on the autoignition regimes in the ξ–ε diagram for H_2/air mixtures.

mixture composition (fuel and equivalence ratio) is still not clear. This deserves further study.

4. Conclusions

Autoignitive reaction front propagation and detonation development from a hot spot in hydrogen/air mixtures are investigated numerically. Detailed chemistry is considered in simulations. Five modes and their regimes are identified in the plot based on two non-dimensional parameters, ξ and ε. The coherent coupling between pressure wave and chemical reaction can induce detonation development. It is found that the detonation development regime is fuel-dependent and thereby the detonation peninsula of Bradley and coworkers [12,21] might not work for all fuels. Besides, different shapes of detonation development regime are observed for different values of initial pressure, initial temperature and equivalence ratio. The initial pressure, initial temperature, and equivalence ratio all can affect the detonation development regime. Therefore, to achieve the quantitative prediction of engine knock, we need use the detonation development regime for specific fuel at specific initial pressure, initial temperature, and equivalence ratio.

It is noted that 1D simulation is conducted here. In practical SIEs, the combustion and autoignition are three-dimensional with turbulence. The effects of 3D turbulence on autoignition and detonation development deserve further study.

Acknowledgements

We acknowledge the helpful discussions with Dr. Chengken Qi at Peking University and Professor Yiguang Ju at Princeton University.

Disclosure statement

No potential conflict of interest was reported by the authors.

Funding

This work was supported by National Natural Science Foundation of China [grant numbers 91741126 and 51861135309].

ORCID

Zheng Chen http://orcid.org/0000-0001-7341-6099

References

[1] J.B. Heywood, *Internal Combustion Engine Fundamentals*, McGraw Hill, New York, 1988.
[2] D. Bradley, *'Hot spots' and gasoline engine knock*. J. Chem. Soc. Faraday T. 92 (1996), pp. 2959–2964.
[3] C. Dahnz and U. Spicher, *Irregular combustion in supercharged spark ignition engines – pre-ignition and other phenomena*. Int. J. Engine Res. 11 (2010), pp. 485–498.
[4] G.T. Kalghatgi and D. Bradley, *Pre-ignition and 'super-knock' in turbo-charged spark-ignition engines*. Int. J. Engine Res. 13 (2012), pp. 399–414.
[5] G.T. Kalghatgi, *Developments in internal combustion engines and implications for combustion science and future transport fuels*. Proc. Combust. Inst. 35 (2015), pp. 101–115.
[6] Z. Wang, Y.L. Qi, X. He, J.X. Wang, S.J. Shuai, and C.K. Law, *Analysis of pre-ignition to super-knock: Hotspot-induced deflagration to detonation*. Fuel 144 (2015), pp. 222–227.
[7] Z. Wang, H. Liu, T. Song, Y. Qi, X. He, S. Shuai, and J. Wang, *Relationship between super-knock and pre-ignition*. Int. J. Engine Res. 16 (2015), pp. 166–180.
[8] Z. Wang, H. Liu, and R.D. Reitz, *Knocking combustion in spark-ignition engines*. Prog. Energy Combust. Sci. 61 (2017), pp. 78–112.
[9] G. Kalghatgi, *Knock onset, knock intensity, superknock and preignition in spark ignition engines*. Int. J. Engine Res. 19 (2018), pp. 7–20.
[10] J.H.S. Lee, R. Knystautas, and N. Yoshikawa, *Photochemical initiation of gaseous detonations*. Acta Astronaut. 5 (1978), pp. 971–982.
[11] Y.B. Zeldovich, *Regime classification of an exothermic reaction with nonuniform initial conditions*. Combust. Flame 39 (1980), pp. 211–214.
[12] X.J. Gu, D.R. Emerson, and D. Bradley, *Modes of reaction front propagation from hot spots*. Combust. Flame 133 (2003), pp. 63–74.
[13] L. He and P. Clavin, *Critical conditions for detonation initiation in cold gaseous mixtures by nonuniform hot pockets of reactive gases*. Proc. Combust. Inst. 24 (1992), pp. 1861–1867.
[14] H.J. Weber, A. Mack, and P. Roth, *Combustion and pressure wave interaction in enclosed mixtures initiated by temperature nonuniformities*. Combust. Flame 97 (1994), pp. 281–295.
[15] A.M. Bartenev and B.E. Gelfand, *Spontaneous initiation of detonations*. Prog. Energy Combust. Sci. 26 (2000), pp. 29–55.
[16] A.K. Kapila, D.W. Schwendeman, J.J. Quirk, and T. Hawa, *Mechanisms of detonation formation due to a temperature gradient*. Combust. Theory Model. 6 (2002), pp. 553–594.
[17] G.J. Sharpe and M. Short, *Detonation ignition from a temperature gradient for a two-step chain-branching kinetics model*. J. Fluid Mech. 476 (2003), pp. 267–292.
[18] M.D. Kurtz and J.D. Regele, *Acoustic timescale characterisation of a one-dimensional model hot spot*. Combust. Theor. Model. 18 (2014), pp. 532–551.

[19] D.R. Kassoy, *The response of a compressible gas to extremely rapid transient, spatially resolved energy addition: An asymptotic formulation*. J. Eng. Math. 68 (2010), pp. 249–262.
[20] D.R. Kassoy, J.A. Kuehn, M.W. Nabity, and J.F. Clarke, *Detonation initiation on the microsecond time scale: DDTs*. Combust. Theor. Model. 12 (2008), pp. 1009–1047.
[21] D. Bradley, C. Morley, X.J. Gu, and D.R. Emerson, *Amplified pressure waves during autoignition: Relevance to CAI engines, SAE-2002-01-2868, 2002 (2002)*.
[22] L. Bates and D. Bradley, *Deflagrative, auto-ignitive, and detonative propagation regimes in engines*. Combust. Flame 175 (2017), pp. 118–122.
[23] D. Bradley and G.T. Kalghatgi, *Influence of autoignition delay time characteristics of different fuels on pressure waves and knock in reciprocating engines*. Combust. Flame 156 (2009), pp. 2307–2318.
[24] J. Rudloff, J.M. Zaccardi, S. Richard, and J.M. Anderlohr, *Analysis of pre-ignition in highly charged SI engines: Emphasis on the auto-ignition mode*. Proc. Combust. Inst. 34 (2013), pp. 2959–2967.
[25] A. Robert, S. Richard, O. Colin, and T. Poinsot, *LES study of deflagration to detonation mechanisms in a downsized spark ignition engine*. Combust. Flame 162 (2015), pp. 2788–2807.
[26] L. Bates, D. Bradley, G. Paczko, and N. Peters, *Engine hot spots: Modes of auto-ignition and reaction propagation*. Combust. Flame 166 (2016), pp. 80–85.
[27] P. Dai, C.K. Qi, and Z. Chen, *Effects of initial temperature on autoignition and detonation development in dimethyl ether/air mixtures with temperature gradient*. Proc. Combust. Inst. 36 (2017), pp. 3643–3650.
[28] A. Robert, J.-M. Zaccardi, C. Dul, A. Guerouani, and J. Rudloff, *Numerical study of auto-ignition propagation modes in toluene reference fuel–air mixtures: Toward a better understanding of abnormal combustion in spark-ignition engines*. Int. J. Engine Res. 20 (2018), pp. 734–745.
[29] A. Guerouani, A. Robert, and J.M. Zaccardi, *Detonation Peninsula for TRF-air mixtures: Assessment for the analysis of auto-ignition events in spark-ignition engines, SAE (2018) 2018-01-1721k*.
[30] P. Dai, Z. Chen, and X.H. Gan, *Autoignition and detonation development induced by a hot spot in fuel-lean and CO2 diluted n-heptane/air mixtures*. Combust. Flame 201 (2019), pp. 208–214.
[31] J.Y. Pan, S. Dong, H.Q. Wei, T. Li, G.Q. Shu, and L. Zhou, *Temperature gradient induced detonation development inside and outside a hot spot for different fuels*. Combust. Flame 205 (2019), pp. 269–277.
[32] C.K. Qi, P. Dai, H. Yu, and Z. Chen, *Different modes of reaction front propagation in n-heptane/air mixture with concentration non-uniformity*. Proc. Combust. Inst. 36 (2017), pp. 3633–3641.
[33] T.H. Zhang, W.Q. Sun, and Y.G. Ju, *Multi-scale modeling of detonation formation with concentration and temperature gradients in n-heptane/ air mixtures*. Proc. Combust. Inst. 36 (2017), pp. 1539–1547.
[34] P. Dai and Z. Chen, *Effects of NOx addition on autoignition and detonation development in DME/air under engine-relevant conditions*. Proc. Combust. Inst. 37 (2019), pp. 4813–4820.
[35] Z. Chen, M.P. Burke, and Y.G. Ju, *Effects of Lewis number and ignition energy on the determination of laminar flame speed using propagating spherical flames*. Proc. Combust. Inst. 32 (2009), pp. 1253–1260.
[36] Z. Chen, *Effects of radiation and compression on propagating spherical flames of methane/air mixtures near the lean flammability limit*. Combust. Flame 157 (2010), pp. 2267–2276.
[37] P. Dai and Z. Chen, *Supersonic reaction front propagation initiated by a hot spot in n-heptane/air mixture with multistage ignition*. Combust. Flame 162 (2015), pp. 4183–4193.
[38] R.J. Kee, F. Rupley, and J. Miller, *CHEMKIN-II: A FORTRAN chemical kinetics package for the analysis of gas-phase chemical kinetics*, Sandia Report. SAND89-8009B (1993).
[39] P.N. Brown, G.D. Byrne, and A.C. Hindmarsh, *Vode – a variable-coefficient Ode solver*. SIAM J. Sci. Stat. Comput. 10 (1989), pp. 1038–1051.
[40] P. Dai, Z. Chen, S. Chen, and Y. Ju, *Numerical experiments on reaction front propagation in n-heptane/air mixture with temperature gradient*. Proc. Combust. Inst. 35 (2015), pp. 3045–3052.
[41] Z. Chen, *On the accuracy of laminar flame speeds measured from outwardly propagating spherical flames: Methane/air at normal temperature and pressure*. Combust. Flame 162 (2015), pp. 2442–2453.

[42] M. Faghih and Z. Chen, *The constant-volume propagating spherical flame method for laminar flame speed measurement*. Sci. Bull. 61 (2016), pp. 1296–1310.
[43] Z. Chen, *Effects of radiation absorption on spherical flame propagation and radiation-induced uncertainty in laminar flame speed measurement*. Proc. Combust. Inst. 37 (2017), pp. 1129–1136.
[44] Z. Chen, *Effects of radiation on large-scale spherical flame propagation*. Combust. Flame 183 (2017), pp. 66–74.
[45] C.K. Qi and Z. Chen, *Effects of temperature perturbation on direct detonation initiation*. Proc. Combust. Inst. 36 (2017), pp. 2743–2751.
[46] M. Faghih and Z. Chen, *Two-stage heat release in nitromethane/air flame and its impact on laminar flame speed measurement*. Combust. Flame 183 (2017), pp. 157–165.
[47] M. Faghih, W. Han, and Z. Chen, *Effects of Soret diffusion on premixed flame propagation under engine-relevant conditions*. Combust. Flame 194 (2018), pp. 175–179.
[48] Y. Wang, W. Han, and Z. Chen, *Effects of fuel stratification on ignition kernel development and minimum ignition energy of n-decane/air mixtures*. Proc. Combust. Inst. 37 (2019), pp. 1623–1630.
[49] Z.S. Li, X.L. Gou, and Z. Chen, *Effects of hydrogen addition on non-premixed ignition of iso-octane by hot air in a diffusion layer*. Combust. Flame 199 (2019), pp. 292–300.
[50] M.A. Liberman, A.D. Kiverin, and M.F. Ivanov, *Regimes of chemical reaction waves initiated by nonuniform initial conditions for detailed chemical reaction models*. Phys. Rev. E 85 (2012), pp. 056312-1–11.
[51] C. Wang, C.G. Qian, J.N. Liu, and M.A. Liberman, *Influence of chemical kinetics on detonation initiating by temperature gradients in methane/air*. Combust. Flame 197 (2018), pp. 400–415.
[52] M.A. Liberman, C. Wang, C.G. Qian, and J.N. Liu, *Influence of chemical kinetics on spontaneous waves and detonation initiation in highly reactive and low reactive mixtures*. Combust. Theor. Model. 23 (2019), pp. 467–495.
[53] J. Li, Z.W. Zhao, A. Kazakov, and F.L. Dryer, *An updated comprehensive kinetic model of hydrogen combustion*. Int. J. Chem. Kinet. 36 (2004), pp. 566–575.
[54] M.P. Burke, M. Chaos, Y. Ju, F.L. Dryer, and S.J. Klippenstein, *Comprehensive H2/O2 kinetic model for high-pressure combustion*. Int. J. Chem. Kinet. 44 (2012), pp. 444–474.
[55] A. Keromnes, W.K. Metcalfe, K.A. Heufer, N. Donohoe, A.K. Das, C.J. Sung, J. Herzler, C. Naumann, P. Griebel, O. Mathieu, M.C. Krejci, E.L. Petersen, W.J. Pitz, and H.J. Curran, *An experimental and detailed chemical kinetic modeling study of hydrogen and syngas mixture oxidation at elevated pressures*. Combust. Flame 160 (2013), pp. 995–1011.
[56] V.A. Alekseev, M. Christensen, and A.A. Konnov, *The effect of temperature on the adiabatic burning velocities of diluted hydrogen flames: A kinetic study using an updated mechanism*. Combust. Flame 162 (2015), pp. 1884–1898.
[57] Z. Zhao, Z. Chen, and S. Chen, *Correlations for the ignition delay times of hydrogen/air mixtures*. Chin. Sci. Bull. 56 (2011), pp. 215–221.
[58] Y.L. Qi, Z. Wang, J.X. Wang, and X. He, *Effects of thermodynamic conditions on the end gas combustion mode associated with engine knock*. Combust. Flame 162 (2015), pp. 4119–4128.
[59] Y. Ju, W. Sun, M.P. Burke, X. Gou, and Z. Chen, *Multi-timescale modeling of ignition and flame regimes of n-heptane-air mixtures near spark assisted homogeneous charge compression ignition conditions*. Proc. Combust. Inst. 33 (2011), pp. 1245–1251.
[60] J.B. Martz, H. Kwak, H.G. Im, G.A. Lavoie, and D.N. Assanis, *Combustion regime of a reacting front propagating into an auto-igniting mixture*. Proc. Combust. Inst. 33 (2011), pp. 3001–3006.
[61] A. Krisman, E.R. Hawkes, and J.H. Chen, *The structure and propagation of laminar flames under autoignitive conditions*. Combust. Flame 188 (2018), pp. 399–411.
[62] M. Faghih, H.Y. Li, X.L. Gou, and Z. Chen, *On laminar premixed flame propagating into autoigniting mixtures under engine-relevant conditions*. Proc. Combust. Inst. 37 (2019), pp. 4673–4680.
[63] A. Ansari, J. Jayachandran, and F.N. Egolfopoulos, *Parameters influencing the burning rate of laminar flames propagating into a reacting mixture*. Proc. Combust. Inst. 37 (2019), pp. 1513–1520.
[64] S. Desai, R. Sankaran, and H.G. Im, *Unsteady deflagration speed of an auto-ignitive dimethyl-ether (DME)/air mixture at stratified conditions*. Proc. Combust. Inst. 37 (2019), pp. 4717–4727.

[65] H. Yu and Z. Chen, *End-gas autoignition and detonation development in a closed chamber*. Combust. Flame 162 (2015), pp. 4102–4111.
[66] H. Terashima and M. Koshi, *Mechanisms of strong pressure wave generation in end-gas autoignition during knocking combustion*. Combust. Flame 162 (2015), pp. 1944–1956.
[67] H. Yu, C. Qi, and Z. Chen, *Effects of flame propagation speed and chamber size on end-gas autoignition*. Proc. Combust. Inst. 36 (2017), pp. 3533–3541.
[68] H. Terashima, A. Matsugi, and M. Koshi, *Origin and reactivity of hot-spots in end-gas autoignition with effects of negative temperature coefficients: Relevance to pressure wave developments*. Combust. Flame 184 (2017), pp. 324–334.
[69] H. Terashima, A. Matsugi, and M. Koshi, *End-gas autoignition behaviors under pressure wave disturbance*. Combust. Flame 203 (2019), pp. 204–216.